Author postprint of the paper published in Journal of Alloys and Compounds 611 (2014) 427–432

Structural, magnetic and magneto-transport properties of monovalent doped manganite $Pr_{0.55}K_{0.05}Sr_{0.4}MnO_3$

R. Thaljaoui [a,b,c],W. Boujelben[a], M. Pękała[c], K. Pękała[b], J. Antonowicz [b], J.-F. Fagnard[d], Ph. Vanderbemden[d], S. Dąbrowska[e], J. Mucha[f]

(a) Laboratoire de Physique des Matériaux, Faculté des Sciences de Sfax, Université de Sfax, B. P. 1171, 3000 Sfax, Tunisia.
(b) Faculty of Physics, Warsaw University of Technology, Koszykowa 75, 00-662 Warsaw, Poland.
(c) Department of Chemistry, University of Warsaw, Al. Zwirki i Wigury 101, 02-089, Poland.
(d) SUPRATECS, Department of Electrical Engineering and Computer Science (B28), University of Liege, Belgium.
(e) Warsaw University of Technology, Faculty of Materials Science, ul. Wołoska 141 02-507 Warsaw, Poland.
(f) Institute of Low Temperature Physics and Structural Research, 50-422 Wrocław, Poland

Abstract

$Pr_{0.55}K_{0.05}Sr_{0.4}MnO_3$ sample have been synthesized using the conventional solid state reaction. Rietveld refinements of the X-ray diffraction patterns at room temperature confirm that the sample is single phase and crystallizes in the orthorhombic structure with P*nma* space group; the crystallite size is around 70 nm. The SEM images show that grain size spreads around 1000 - 1200 nm. DTA analysis do not reveal any clear transition in temperature range studied. The low-temperature DSC indicates that Curie temperature is around 297 K. Magnetization measurements in a magnetic applied field of 0.01 T exhibit a paramagnetic-ferromagnetic transition at the Curie temperature T_C = 303 K. A magnetic entropy change under an applied magnetic field of 2 T is found to be 2.26 J kg^{-1} K^{-1}, resulting in a large relative cooling power around 70 J/kg. Electrical resistivity measurements reveal a transition from semiconductor to metallic phase. The thermal conductivity is found to be higher than that reported for undoped and Na doped manganites [1].

Introduction

Perovskite manganites with general formula $R_{1-x}T_xMnO_3$ where R is a rare earth atom (La, Pr, Nd, ..) amd T is an alkaline earth elemnt (Sr, Ca, Ba,..), have been attracted much renewed attention. Such interrest is mainly related to the discovery of the colossal magnetoresistance (CMR) in these materials. In fact, physical properties of ferromagnetic mixed-valence manganites are strongly influenced by the application of an external magnetic field resulting in a decrease of the electrical resistivity around their metal-insulator transition temperature T_{MI} and giving rise to CMR effect [2]. The complex manganite phenomena, has been explained by using many theories, such as the double exchange theory, Jahn-Teller effect, polaronic effect and phase separation [3-5], but still complicate. In these manganites systems a simple chemical substitution in A-site leads to a mixed Mn^{3+}/Mn^{4+} valence resulting the ferromagnetic interaction controlled by the hopping of e_g electron between Mn^{3+} and Mn^{4+} ions via the orbital overlap 2p [6]. In fact, the physical properties of manganites are mainly controlled by the ratio between Mn^{3+} and Mn^{4+} ions, the average size and the degree of disorder at the A-site. Recently, Rocco et al. [7] confirm the direct relationship between the average ionic radius, the MCE and the Curie temperature. The materials required for magnetic refrigeration exhibit large magnetocaloric effect around their phase transition temperature. Generally, the MCE values for manganite are related to their phase transitions orders and the highest values were reported for that with first order transition [8]. Moreover, the manganites are relatively cheap and easy for technological treatments.

There is a growing research activity devoted to hole doped manganites with monovalent metals [9-11]. In fact the substitution with monovalent metals converts more Mn^{3+} ions to Mn^{4+} compared to divalent metals due to valence difference. Recently, Li et al. [9] report the coexistence of large magnetoresistance and magnetocaloric effect in monovalent doped manganite $La_{0.5}Ca_{0.4}Li_{0.1}MnO_3$. Previously, we have reported with details the studies of K-doped compounds $Pr_{0.6}Sr_{0.4-x}K_xMnO_3$ [11] and it was found that ferromagnetic-paramagnetic transition temperature (T_C) decreases from 310 K to 269 K with increasing K concentration from 0 up to 0.2, and the metal-insulator transition temperature T_{MI} exhibits a slight decrease from 184 K down to 170 K, when K concentration x increases from 0 to 0.1 [12]. On contrary, for $Pr_{0.55}Na_{0.05}Sr_{0.4}MnO_3$ manganite [1], both transition temperatures were 289 K and 104 K for T_C and T_{MI}, respectively which represents a significant decrease compared to that reported for parent sample $Pr_{0.6}Sr_{0.4}MnO_3$ [12]. To our knowledge there has not been any report on physical properties of $Pr_{0.55}K_{0.05}Sr_{0.4}MnO_3$ manganite previously. This motivates us to extend our recent studies on monovalent doped manganites and we report new investigations summarizing the effect of 5% K doping in Pr-site in $Pr_{0.6}Sr_{0.4}MnO_3$ manganite on structural, magnetic, magneto caloric, electrical and thermal conductivity properties.

Experimental details

$Pr_{0.55}K_{0.05}Sr_{0.4}MnO_3$ sample were prepared by using the standard conventional solid state reaction method as described previously [11, 12]. Homogeneity and cell parameters were studied by the X-ray diffraction with Cu-Kα radiation (1.54 Å) in the 2θ range of 10 - 100 degrees. Structural analysis was carried out using the standard Rietveld technique [13, 14]. In order to check thermal stability, simultaneous DSC and TGA analysis was performed using Q600 (TA instruments) apparatus operating under high purity argon flow of 100 ml/min. The measurements were performed during constant heating at 20 °C/min from room temperature up to 1350 °C for a sample of 47 mg. The density was measured using AccuPycII 1340 helium pycnometer. The morphology and grain size distribution were studied by SEM (Scanning Electron Microscopy). The magnetic measurements were carried out using PPMS (Physical Property Measurement System from Quantum Design) in applied magnetic field up to 2 T. The temperature variation of electrical resistivity was measured by the four probe method. The thermal conductivity was measured using the stationary heat flux method in the temperature range 5 K - 300 K [1].

Structure

The X-ray diffraction patterns recorded at room temperature (Fig. 1) confirm that manganite is a single phase crystallizing in the orthorhombic structure with *Pnma* space group. Using Rietveld refinement, lattice parameters are calculated to be equal to 5.43884(2) Å, 7.6566(2) Å and 5.48313(1) Å for a, b and c, respectively. The unit cell volume of 228.334 $Å^3$ is found to be slightly smaller than 229.295 $Å^3$ reported for undoped manganite $Pr_{0.6}Sr_{0.4}MnO_3$ [10, 15]. Such a volume decrease can be explained by the increase of the Mn^{4+} content with average ionic radius (0.53 Å) on the cost of the Mn^{3+} content with average ionic radius (0.65 Å) [16]. This correlates with the theoretical expression:

$$\mathrm{Pr}^{3+}_{0.6-x}\,K^{+}_{x}\,Sr^{2+}_{0.4}\,Mn^{3+}_{0.6-2x}\,Mn^{4+}_{0.4+2x}\,O^{2-}_{3} \qquad (1)$$

The 5% K doping in Pr -site induces an increase in Mn^{4+} fraction from 0.4 to 0.5.

The average crystallite size was evaluated from a width of diffraction peaks using Scherrer formula: $C_{XRD} = \dfrac{K * \lambda}{\beta * COS\theta}$ (2)

where K is the Scherrer constant , λ is the X-ray wave length, Θ and β are the Bragg angle and the width at half maximum of the XRD peak, respectively. The obtained value is 70 nm. The mean grain size value G_{SEM} was estimated from SEM images shown in Fig. 2. One can notice that the grains are irregularly spherical like and the mean size is varying between 1 and 1.2 μm. The agglomeration degree defined by the ratio G_{SEM}/C_{XRD} is about 15. The significant difference between G_{SEM} and C_{XRD} confirms that the grains observed by SEM consist of several crystallites [17].

Differential thermal / thermogravimetric analysis (DTA/TGA) did not reveal any clear transition in temperature range studied. The observed signal variation is ascribed mainly to the baseline drift. Simultaneously measured TGA signal (Fig. 3A) shows that sample mass decreases slowly by 0.3 % up to 1200 °C and drops more rapidly down to 99.4% of initial mass at 1350 °C. In order to determine Curie temperature a differential scanning calorimetry (DSC) analysis was carried out with DSC Q200 apparatus (TA Instruments) equipped with refrigerating cooling system RCS90. Powdered sample (37 mg) was sealed inside aluminum pan, placed inside the DSC cell operating under high-purity nitrogen purge flow (50 ml/min) and heated from -80 to 100 °C applying 5 °C/min heating rate. The low-temperature DSC measurements show a clear endothermic peak in the heat flow Fig. 3B (corresponding to C_p maximum) which is a mark of Curie temperature at 297 K.

The manganite density D measured by means of the precise helium method is found to be 6.2106 and 6.2340 (g/cm^3) for undoped ($Pr_{0.6}Sr_{0.4}MnO_3$) and doped manganite ($Pr_{0.55}K_{0.05}Sr_{0.4}MnO_3$), respectively. The XRD density was also calculated according to the following formula:

$$D_{XRD} = ZM/AV \quad (3)$$

where Z, M, A and V correspond to the number of manganite molecules per unit cell, molecular mass, Avogadro number and unit cell volume, respectively. The result was 6.4515 and 6.3125 (g/cm^3) for undoped and doped manganites, respectively. These values are in a range typical for manganites [18]. A comparison of the measured density with the XRD density reveals the relatively low porosity defined as:

$$P = 1 - (D/D_{XRD}) \quad (4)$$

The obtained values are 0.037 and 0.012 for undoped and doped samples, respectively. Such a low porosity gives evidence of the high quality of the well compacted manganite.

Magnetic results

The temperature dependences of DC magnetization measured in zero-field cooling (ZFC) and under field cooling (FC) modes at a magnetic field of 10 mT for $Pr_{0.55}K_{0.05}Sr_{0.4}MnO_3$ sample, shown in Fig. 4, indicate that the two curves coincide at high temperature and start to spread just below the ferromagnetic Curie temperature T_C equal to 303 K: this comparable to the 297 K value deduced from DSC measurements. In fact, DSC and magnetization measurements do not probe the same quantity so, besides the uncertainty of temperature determination, there might be some (small) difference in T_C resulting from both methods. The ZFC plot shows a broad maximum below 300 K and the magnetization decreases with lowering temperature, whereas the FC plot globally increases with decreasing temperature. Such irreversibility effect is related to the domain wall pinning effect. A weak irregularity in magnetization is observed for FC magnetization around 150 K. Similar behaviour was reported for $Pr_{0.55}Na_{0.05}Sr_{0.4}MnO_3$ manganite at 170 K [1], and explained by the structural transition from the high temperature orthorhombic P*nma* to the low temperature monoclinic I_2/a space group. Comparable irregularity was observed at temperature higher than 65 K for $Pr_{0.6}Sr_{0.4}MnO_3$ single crystal [19] and at 40 K for $Pr_{0.6}Sr_{0.4-x}K_xSr_0MnO_3$ [11]. The ferromagnetic Curie temperature T_C = 303 K is reduced by 7 K as compared to the undoped

sample $Pr_{0.6}Sr_{0.4}MnO_3$ [10, 15], and is 13 K higher than that reported for $Pr_{0.55}Na_{0.05}Sr_{0.4}MnO_3$ [1]. The decrease of T_C can be explained by the increase of Mn^{4+}/Mn^{3+} ratio since the 5% K^+ doping in Pr-site enhances Mn^{4+} concentration from 0.4 to 0.5 This results in the reduction of the effective exchange interaction and less overlap between Mn-3d and O-2p orbitals as revealed by the decreasing of T_C value. However, the bandwidth W [20], which may control the magnetic and transport properties, is found weakly decreasing from 0.097 reported for the undoped sample $Pr_{0.6}Sr_{0.4}MnO_3$ [11] to 0.096. The temperature dependence of the in-phase AC magnetic susceptibility $\chi'(T)$ measured under a magnetic field of 1 mT in temperature range 10 K to 340 K is shown in Fig. 5A. The magnetic susceptibility $\chi'(T)$ is a monotonically increasing function of temperature up to just below T_C. The similar susceptibility behaviour was reported previously for similar manganite $Pr_{0.6}Sr_{0.4-x}K_xMnO_3$ [21]. The variation of $\chi'(T)$ confirms the appearance of the magnetic transition. We should also note that the T_C value defined as the minimum of $d\chi'(T)/dt$ is in accordance with that determined from the first derivative of FC magnetization measured and with the T_C value determined by using low temperature DSC measurement described above.

The out-of-phase component of AC magnetic susceptibility $\chi''(T)$ exhibits a maximum about 3 K below T_C and slowly diminishes at lower temperatures as illustrated in Fig. 5B. The same behaviour was also reported in ref [21]. The most abrupt decay is observed on the transition to paramagnetic phase at T_C. This behaviour shows that power losses are most intense around Curie temperature and spread over the whole temperature interval of ferromagnetic phase.

The isothermal magnetization data registered in magnetic fields up to 2 T in temperature range 270 K to 321 K with a step of 3 K indicates that the magnetization M increases most abruptly in weak applied field (< 0.2 T) and then approaches to saturation for $\mu_0 H > 1$ T (Fig. 6). The collected results confirm the typical ferromagnetic behaviour below Curie temperature. In order to check the nature of the magnetic transition the Arrott plots were built according to the formula:

$$\frac{H}{M} = A + BM^2 \qquad (5)$$

The M^2 versus H/M curves plotted in Fig. 7 were used to determine the A and B coefficients which correspond to the intercept and the slope of linear fit, respectively. The temperature dependences of A and B Landau coefficients shown in Fig. 8 indicate the evolution of A parameter from negative to positive values with increasing temperature. The zero value of parameter A is observed at T_C = 303 K. The positive B parameter is characteristic for the second order phase transition according to the Banerjee criterion [22].

Magnetic entropy

The magnetic entropy change ΔS was calculated from isothermal magnetization measurements using thermodynamic Maxwell relation and the standard procedure as described previously [10, 11]. The temperature dependences of the magnetic entropy change ΔS shown in Fig.9 confirm that the magnetic entropy change ΔS originates from single ferro- to paramagnetic phase transition. The obtained magnetic entropy change under an applied magnetic field of 2 T is found to be 2.26 J kg^{-1} K^{-1}. Such a value is noticeably higher as compared to 1.95 J/kg K found for the potassium free manganite $Pr_{0.6}Sr_{0.4}MnO_3$ [10] and smaller than those reported for $Pr_{0.6}Sr_{0.4-x}K_xMnO_3$ sample [11]. The ΔS maximum is located in vicinity of Curie temperature. The half width at a maximum is 31 K.

The magnetic entropy change is known to depend both on temperature T and magnetic field B. This magnetic field dependence of maximum magnetic entropy change ΔS_{MAX} at Curie temperature T_C is usually approximated by the simple formula [23, 24]

$$\Delta S_{MAX}(H) = \text{const } H^N \quad (6)$$

The obtained value of N exponent is equal to 0.75 being compatible to those found for other manganites [10] and transition metal based amorphous alloys (N = 0.75) [25]. The N values are related to critical exponents with the following formula [26]:

$$N = 1 + \frac{\beta - 1}{\gamma + \beta} \quad (7)$$

In the separate work on modified Arrot plots the β and γ values are found to be 0.42 and 1.02, respectively. This results in N = 0.59 which is smaller than that deduced from Eq. (6) and is comparable to N= 2/3 reported by H. Oesterreicher et al. [27].

Cooling power

The so called relative cooling power RCP defined as [28]:

$$RCP = -\Delta S_{MAX}\, \delta T_{FWHM}, \quad (8)$$

was estimated using ΔS_{MAX} as the maximum entropy change and δT_{FWHM} as temperature half width. The obtained RCP value under a magnetic field of 2 T is found to be 70 J/kg which is smaller than 102 J/kg of the parent manganite $Pr_{0.6}Sr_{0.4}MnO_3$ [10]. This RCP reduction occurs due to the narrowing of temperature interval δT, which for ΔB = 2 T shrinks down to about 31 K from 52 K for undoped sample. Similar δT narrowing was reported previously for K doped manganites [11], which compensates the ΔS_{MAX} enhancement. We should also note that RCP values are smaller than those observed for $Pr_{0.6}Sr_{0.4-x}Na_xMnO_3$ manganites [10] exhibiting the roughly twice broader temperature half width accompanied by the reduced ΔS_{MAX}. Such abehaviour can be related to the strong sensitivity of RCP to the microstructure created during various preparation and treatment processes. This pertains mainly the grain sizes of present samples, which are slightly larger than those reported for sodium and potassium samples [10, 11].

The influence of magnetic field on RCP may be estimated according to the formula:

$$RCP(H) = \text{const } H^R \quad (9)$$

The deduced R exponent from the numerical fit of Eq. (9) is equal to 1.003 with accuracy about 0.02. The obtained value is comparable to 1.04 reported for undoped manganite and is smaller than that reported in ref [10, 29].

Electrical resistivity

The temperature dependence of electrical resistivity in zero field and in the field of 1 T is shown in Fig. 10 for a temperature range 20 K - 280 K. The $Pr_{0.55}K_{0.05}Sr_{0.4}MnO_3$ manganite exhibits a semiconductor - metal (SC-M) transition for both applied fields at temperature T_ρ at which the resistivity maximum value is observed. The application of 1 T magnetic field weakly influences T_ρ which is slightly shifted from 194 K to 197 K. Similar behaviour was reported for undoped sample $Pr_{0.6}Sr_{0.4}MnO_3$ [12]. We should note that deduced T_ρ for the present sample is remarkably higher than 104 K to 114 K reported for Na-doped manganite $Pr_{0.6}Sr_{0.35}Na_{0.05}MnO_3$ [1]. We should also note that the absolute value reported at 280 K is about 4.7 mΩ m. This value is found higher than 1.2 to 1.4 mΩ m reported previously for $Pr_{0.6}Sr_{0.4-x}K_xMnO_3$ samples [12] and smaller than 10 mΩ m reported for $Pr_{0.55}Na_{0.05}Sr_{0.4}MnO_3$ manganite [1]. Such difference can be related to the sample morphology. In fact our present sample shows the largest crystallite size of 70 nm, generally a decrease of crystallite size is followed by an increase of surface boundary layer which obviously affects the electrical resistivity. With such small grain size, grain boundaries play a major role. The resistivity magnitude is only weakly influenced by magnetic field at high temperature. The value was

about 4.7 mΩ m at 280 K then reaches a maximum of 6.95 mΩ m with lowering temperature to T_ρ. However, the resistivity curves begin to separate from each other below T_ρ. The spreading of the resistivity magnitude $\Delta\rho = [\rho(0T)-\rho(1T)]$ is increasing from 0.2 to 0.5 mΩ m with temperature decreasing from 170 K to 20 K. It can be related to the charge carriers delocalization induced by the external applied magnetic field which decreases the resistivity and results in the local ordering of spins. One can also note that the deduced semiconductor-metal transition temperature T_ρ located in the temperature range 194 K - 197 K does not coincide with the paramagnetic PM-FM temperature transition which is about 100 K higher. Similar behaviour was reported for other manganites [30]. The relatively high resistivity observed from 20 K to about 190 K is composed of two components. The residual (structural) component is known to arise due to structural and chemical defects. The second, magnetic component is due to electron scattering on spin fluctuations. An application of a 1 T magnetic field suppresses spin fluctuations and the electrical resistivity associated with magnetic disorder becomes reduced. An influence of the magnetic field is given by the magnetoresistance (MR) calculated according to the following formula:

$$MR(T) = \frac{\Delta\rho}{\rho} = \frac{\rho(H) - \rho(0)}{\rho(0)} \qquad (10)$$

where ρ(H) and ρ(0) are the resistivities at magnetic field H and at zero fields, respectively. Fig. 11 shows that the negative MR is the largest (-14 %) at 20 K which is somewhat lower than 17 % and 19 % observed for $Pr_{0.6}Sr_{0.4-x}K_xMnO_3$ [12], and then gradually decreases up to 225 K and then increases. This shows that MR originates from the grain boundary contributions. The magnetic disorder responsible for the magnetic component of resistivity seems to be related to the intergrain or intercrystallite volumes.

Thermal conductivity

Temperature variation of thermal conductivity k (T) of $Pr_{0.55}K_{0.05}Sr_{0.4}MnO_3$ measured between 5 K and 300 K is shown in Fig. 12. The thermal conductivity value rises from 0.25 W $K^{-1}m^{-1}$ at 5 K to 3.18 W $K^{-1}m^{-1}$ at 150 K and then drops to 2.58 at 270 K. The obtained values are higher than those reported for undoped sample $Pr_{0.6}Sr_{0.4}MnO_3$, which varies from 0.2 to 1.8 W $K^{-1}m^{-1}$ at 5 K and 270 K, respectively [1]. We should also note that the substitution of 5 % potassium shows a higher thermal conductivity value than doped sample with same content of sodium [1]. However Daivajna et al. [31] reported low values which lie in the range of 0.5 - 4.5 W $K^{-1}m^{-1}$ for $Pr_{0.6-x}Bi_xSr_{0.4}MnO_3$ manganites and they related the result to the presence of JT distortion in these manganite. The highest values of thermal conductivity reported for the present sample compared to that published previously [1], can be explained by the largest crystallite sizes 70 nm which is somewhat higher than 51 nm reported for Na-doped sample [10].

Conclusion

In summary, we have explored the effect of 5 % K doping in Pr-site in $Pr_{0.6}Sr_{0.4}MnO_3$ manganite on physical properties. Structural studies confirms that present sample is single phased with P*nma* space group, the mean crystallite size is about 70 nm and grain size spreads around 1 μm. DTA analysis indicates the stability of the sample transition in studied temperature. The magnetic results indicate that it displays a second order phase transition at 303 K and possesses considerable magnetic entropy change of 2.26 J kg^{-1} K^{-1} resulting RCP value of 70 J/kg for an applied magnetic field of 2 T. The electrical measurements indicate a metallic to semiconductor phase transition at 194 K and a negative magnetoresistance, reaching 14 % at 25 K and gradually decaying with increasing temperature, related to grain boundaries. Thermal conductivity results indicate that reported values are higher than those

reported for undoped and Na- doped samples [1], which can be explained by the largest crystallite sizes 70 nm reported for the present sample.

Acknowledgements. This work was supported in parts by the Tunisian Ministry of Higher Education and Scientific Research, by the Polish Government, by WBI (Belgium) in a frame of scientific exchange agreement and This work has been supported by the European Union in the framework of European Social Fund through the Warsaw University of Technology Development Programme. Authors are grateful to Dr. hab. M. Donten, Ph.D. and Marianna Gniadek for kindly providing electron micrographs and dr Mirosław Salamończyk for X-ray diffraction studies.

References

[1] R. Thaljaoui, W. Boujelben, M. Pękała, K. Pękała, J. Mucha, A. Cheikhrouhou, Cheikhrouhou, J. Alloys Compd. 558 (2013) 236.
[2] J.M.D. Coey, M. Viret, S. von Molnar, Adv. Phys. 48 (1999) 167; M.B. Salamon, M. Jaime, Rev. Mod. Phys. 73 (2001) 583.
[3] A. J Millis, P. B Littlewood, and B. I.Shraiman, Phys. Rev. Lett. 74 (1995) 5144.
[4] A. J. Millis, Phys. Rev. B 53 (1996) 8434.
[5] S. Mori, C. H. Chen, S. W. Cheong, Phys. Rev. Lett. 81(1998) 3972.
[6] C. Zener, Phys. Rev. 81 (1951) 440.
[7] D. L. Rocco,1 A. A. Coelho, 2 S. Gama, 3 and M. de C. Santos, J. Appl. Phys. 113 (2013) 113907.
[8] N. S. Bingham, P. J. Lampen, T.-L. Phan, M.-H. Phan, S.-C. Yu, and H. Srikanth, J. Appl. Phys. 111 (2012) 07D705.
[9] Renwen, Wei Tong, LiPi, Yuheng Zhang, J. Magn. Magn. Mater 355 (2014) 276.
[10] R. Thaljaoui, W. Boujelben, M. Pękała, K. Pękała, W. Cheikhrouhou-Koubaa, A. Cheikhrouhou, J. Mater. Sci. 48 (2013) 3894.
[11] R. Thaljaoui , W. Boujelben, M. Pękała, K. Pękała, J.-F. Fagnard, P. Vanderbemden, M. Donten, A. Cheikhrouhou, J. Magn. Magn. Mater 352 (2014) 6.
[12] R. Thaljaoui, W. Boujelben, M. Pękała, K. Pękała, A. Cheikhrouhou, J. Supercond. Nov. Magn. 26 (2013) 1625.
[13] H.M. Rietveld, J. Appl. Cryst. 2 (1969) 65.
[14] T. Roisnel, J. Rodriguez-Carvajal, Computer program FULLPROF, LLB-LCSIM. May 2003.
[15] R. Thaljaoui, W. Boujelben, M. Pękała, D. Pociecha, J. Szydłowska, A. Cheikhrouhou, J. Alloys Comp. 530 (2012) 138.
[16] R.D. Shanon, Acta. Cryst. A 32 (1976) 751.
[17] S. Das, T.K. Dey, J. Phys. D: Appl. Phys. 40 (2007) 185.
[18] G. Lalitha, P. Venugopal Reddy, J. Magn. Magn. Mater 320 (2008) 754.
[19] S. Roessler, Harikrishnan S. Nair, U. K. Roessler, C.M.N. Kumar, Suja Elizabeth, and S. Wirth, Phys. Rev. B 84 (2011) 184422.
[20] P.G. Radaelli, G. Iannone, M. Marezio, H.Y. Hwang, S.-W. Cheong, J.D. Jorgensen, D.N. Argyriou, Phys. Rev. B 56 (1997) 8265.
[21] R. Thaljaoui, K. Pękała, M. Pękała, W. Boujelben, J. Szydłowska , J.-F. Fagnard, P. Vanderbemden, A. Cheikhrouhou, J. Alloys Comp. 580 (2013) 137.
[22] S.K. Banerjee, Phys. Lett. 12 (1964) 67.
[23] V. Franco, J. S. Blázquez, and A. Conde, Appl. Phys. Lett. 89 (2006) 222512.
[24] M. Pękała, K. Pękała, V. Drozd, K. Staszkiewicz, J.-F. Fagnard, P. Vanderbemden, J. Appl. Phys. 112 (2012) 023906.
[25] Franco V, Blazquez JS, Conde A (2003) Appl Phys Lett 89:222512.

[26]V. Franco, A. Conde, J. M. Romero-Enrique, and J. S. Blazquez, J. Phys.: Condens. Matter 20 (2008) 285207.
[27] H. Oesterreicher and F. T. Parker, J. Appl. Phys. 55 (1984) 4334.
[28] A.M. Tishin, in Handbook of Magnetic Materials, edited by K.H.J. Buschow (Elsevier, Amsterdam, 1999), Vol. 12, p. 395.
[29] V. Franco, J.S. Blázquez, A. Conde, J. Appl. Phys. 103 (2008) 07B316.
[30] R. Mahendiran, R. Mahesh, A.K. Raychaudhuri, C.N.R. Rao, Solid State Commun. 99 (1996) 149.
[31] Mamatha D. Daivajna, Neeraj Kumar, V.P.S. Awana , Bhasker Gahtori, J. Benedict Christopher, S.O. Manjunath, K.Z. Syu, Y.K. Kuo, Ashok Rao, J. Alloys Comp. 588 (2014) 406.

Figures

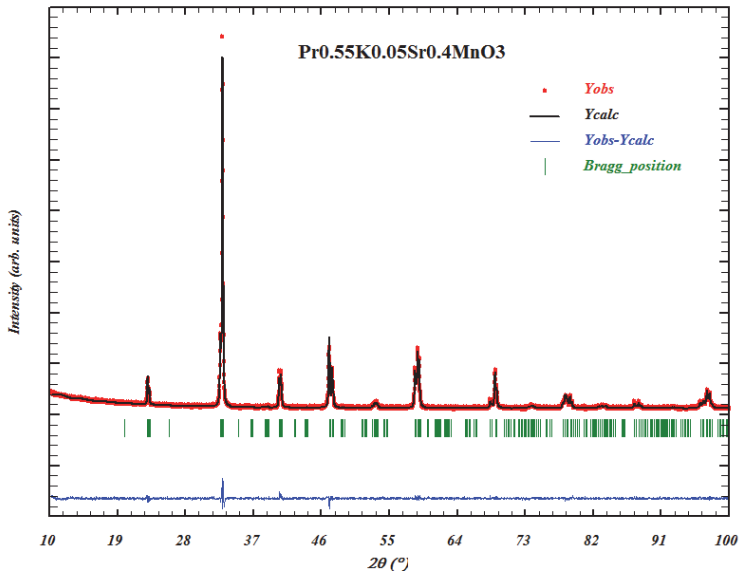

Fig. 1. XRD patterns for $Pr_{0.55}K_{0.05}Sr_{0.4}MnO_3$ manganite.

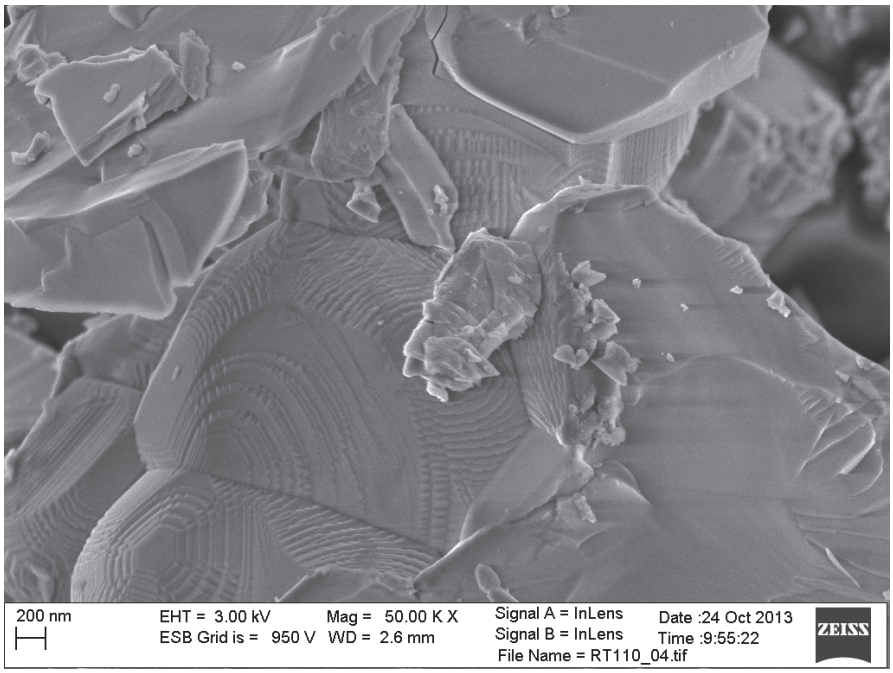

Fig. 2. Scanning electron micrograph of $Pr_{0.55}K_{0.05}Sr_{0.4}MnO_3$ manganite.

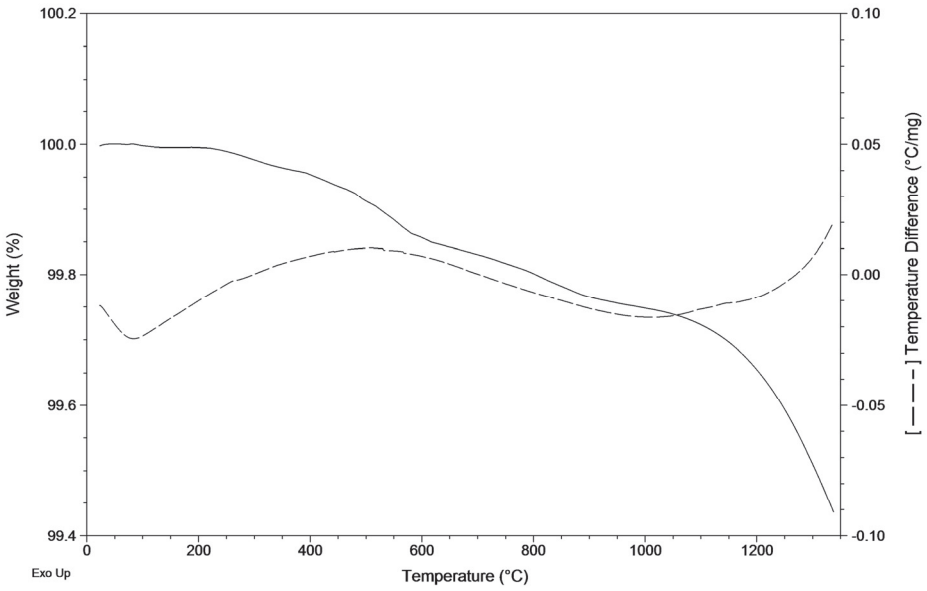

Fig. 3A. The DSC analysis for $Pr_{0.55}K_{0.05}Sr_{0.4}MnO_3$ manganite.

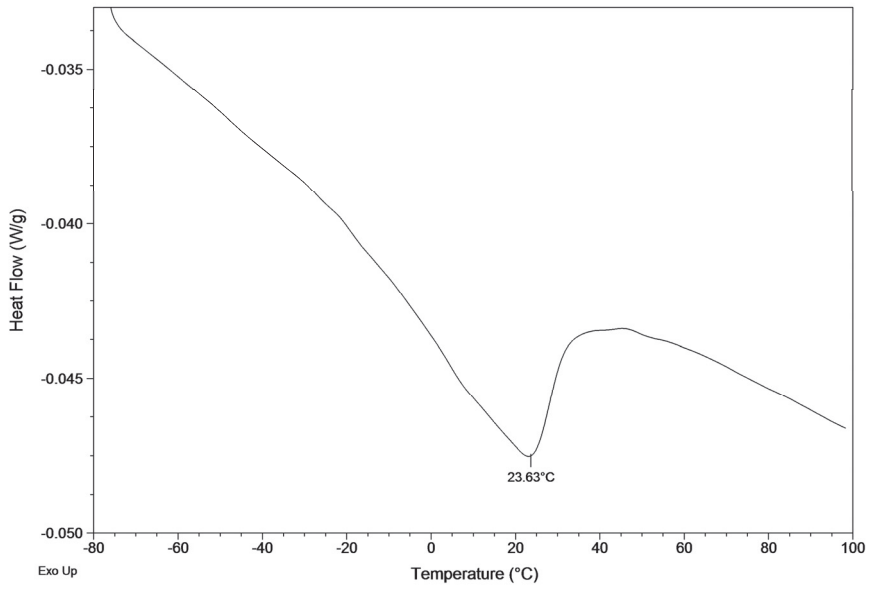

Fig. 3B. The low-temperature DSC analysis for $Pr_{0.55}K_{0.05}Sr_{0.4}MnO_3$ manganite

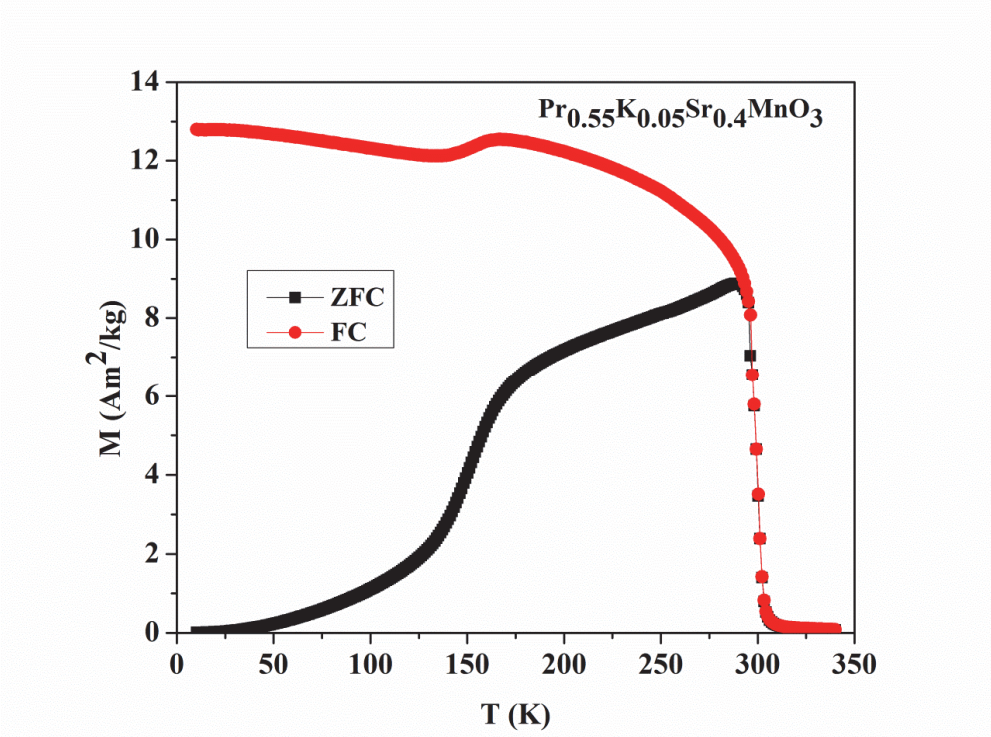

Fig. 4. Temperature variation of zero field cooled (ZFC) and field cooled (FC) magnetization measured at magnetic field of 100 Oe for $Pr_{0.55}K_{0.05}Sr_{0.4}MnO_3$ manganite.

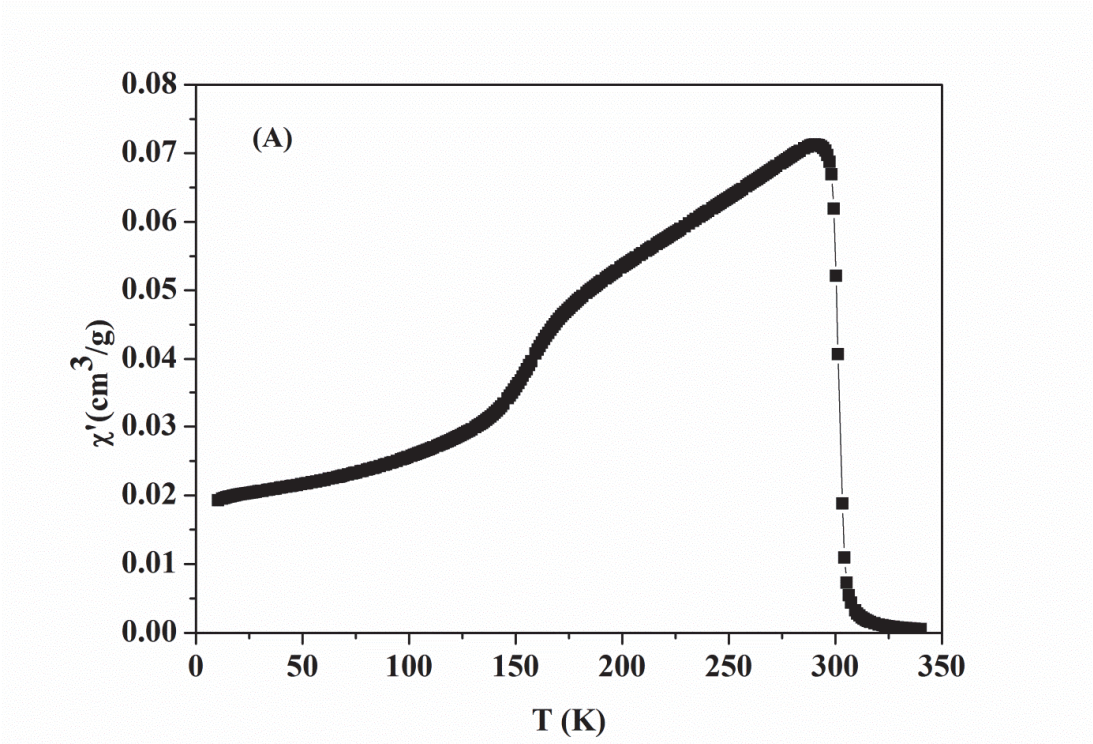

Fig. 5A. Temperature variation of in-phase components of AC magnetic susceptibility for $Pr_{0.55}K_{0.05}Sr_{0.4}MnO_3$ manganite.

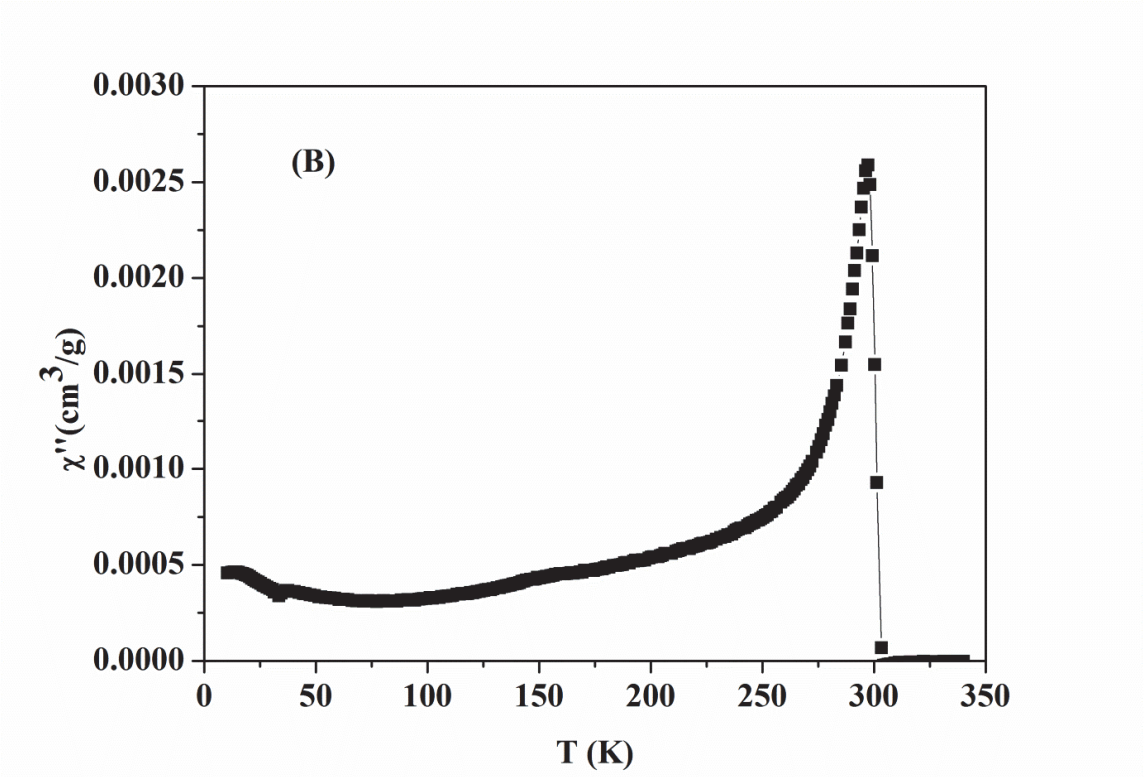

Fig. 5B. Temperature variation of out-of-phase components of AC magnetic susceptibility for $Pr_{0.55}K_{0.05}Sr_{0.4}MnO_3$ manganite.

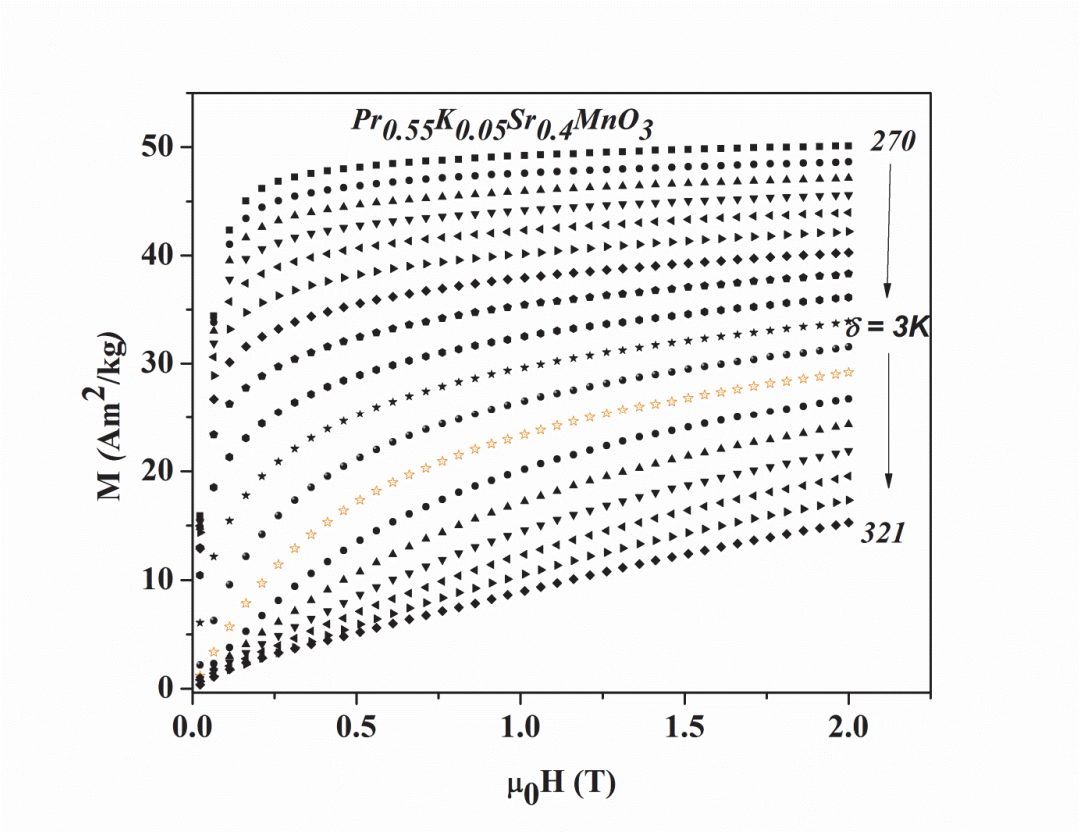

Fig. 6. Magnetization isotherms for $Pr_{0.55}K_{0.05}Sr_{0.4}MnO_3$ manganite.

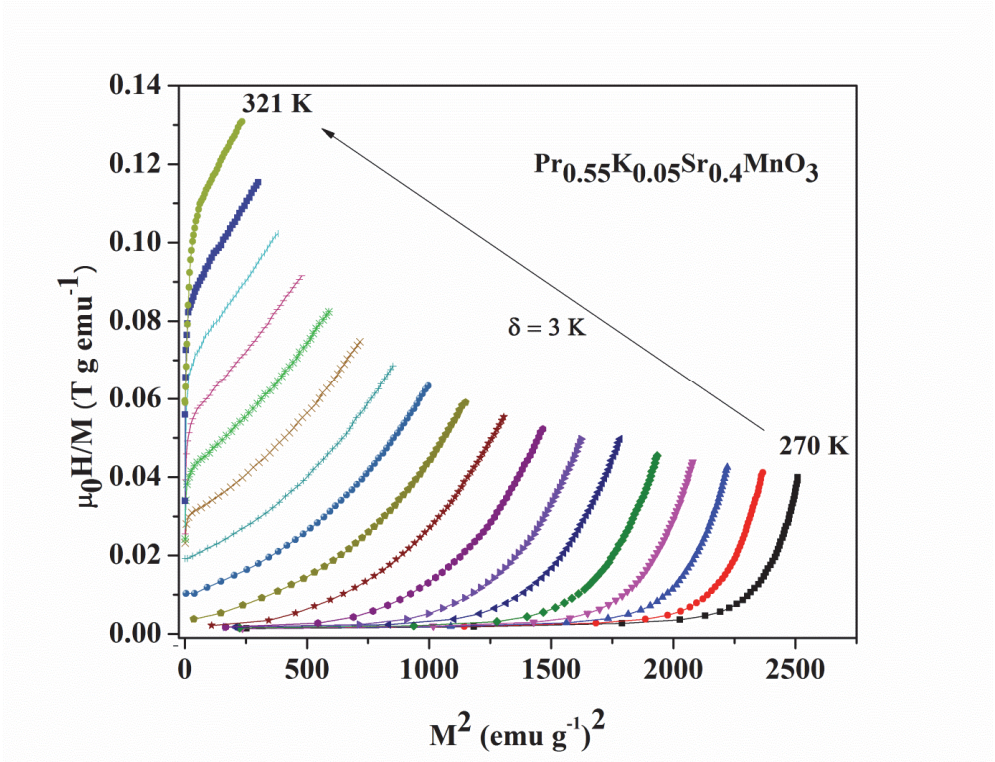

Fig. 7. Arrott plots for $Pr_{0.55}K_{0.05}Sr_{0.4}MnO_3$ manganite.

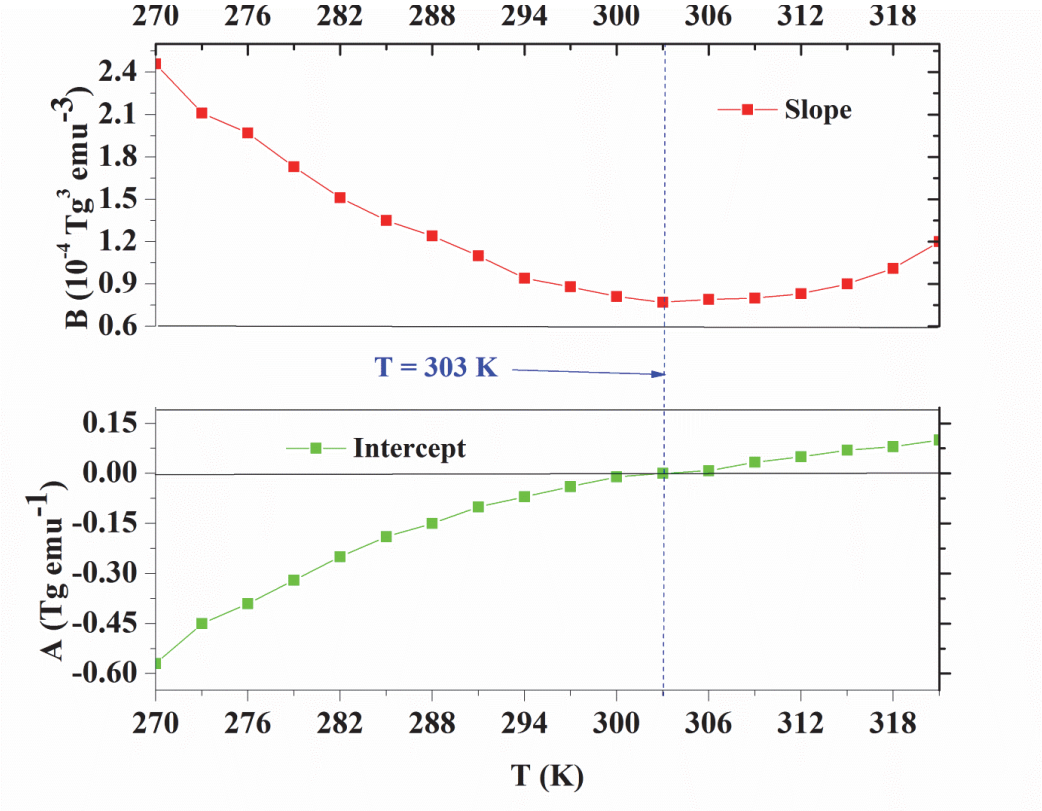

Fig. 8 Temperature dependences of A and B Landau coefficients for $Pr_{0.55}K_{0.05}Sr_{0.4}MnO_3$ manganite.

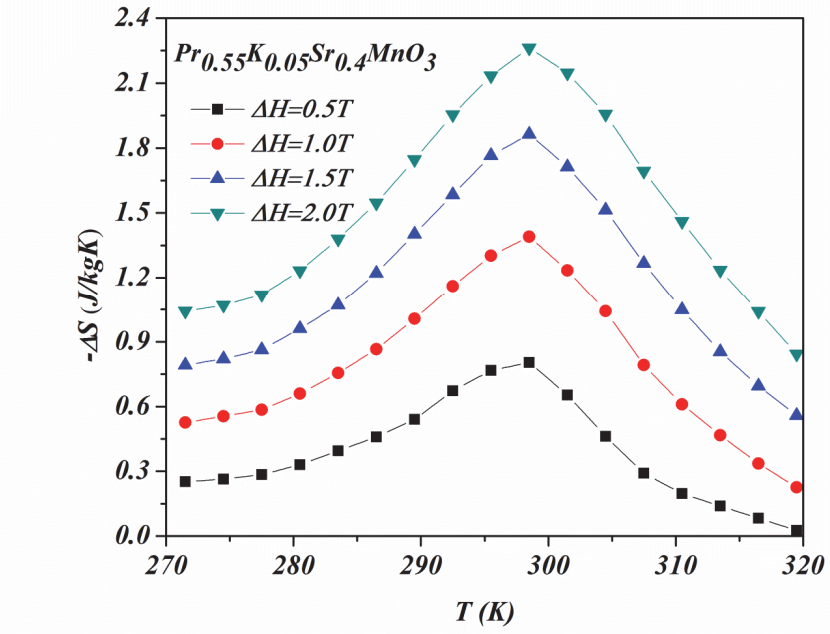

Fig. 9. Temperature variation of magnetic entropy change at various magnetic field change for $Pr_{0.55}K_{0.05}Sr_{0.4}MnO_3$ manganite.

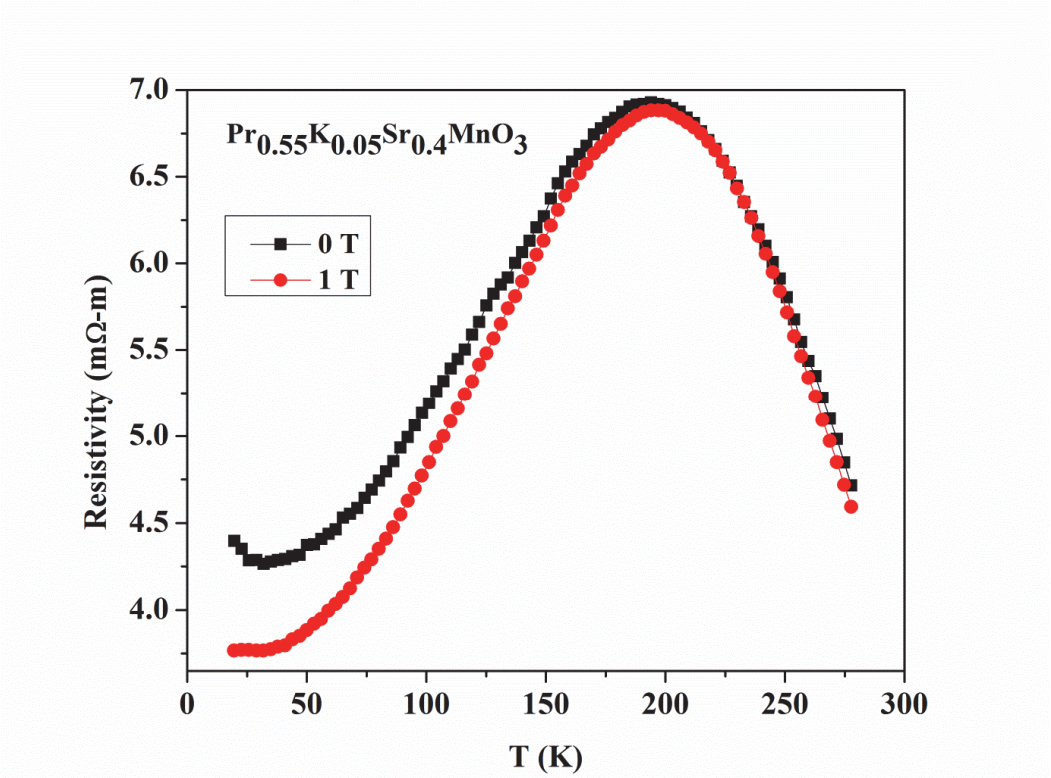

Fig. 10 Temperature variation of electrical resistivity in zero field and in the field of 1T for $Pr_{0.55}K_{0.05}Sr_{0.4}MnO_3$ manganite.

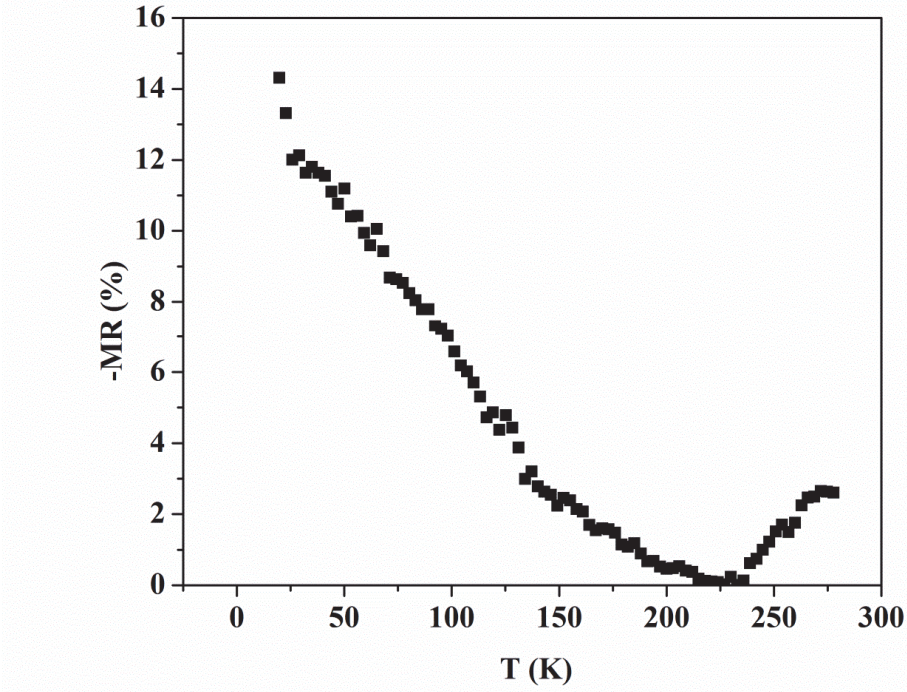

Fig. 11 Temperature variation of magnetoresistance for $Pr_{0.55}K_{0.05}Sr_{0.4}MnO_3$ manganite.

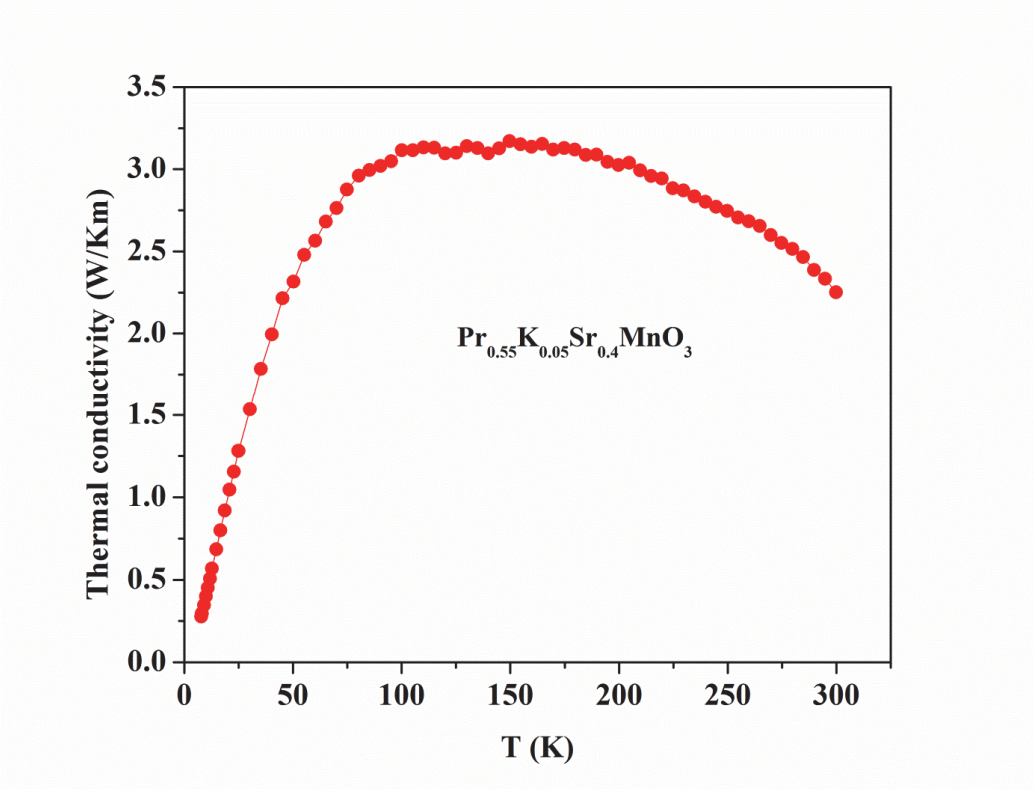

Fig. 12 Temperature variation of thermal conductivity for $Pr_{0.55}K_{0.05}Sr_{0.4}MnO_3$ manganite.